# Supporting Information

## Photovoltaics Driven Ni(II)/Ni(III) Redox Mediator for the Valorization of PET Plastic Waste with Hydrogen Production

Jianying Wang,[a,c,‡] Xin Li,[a,‡] Ting Zhang,[a] Xinyu Chai,[a] Mingze Xu,[c] Menglei Feng,[a] Chengcheng Cai,[a] Zuofeng Chen,[c,*] Xufang Qian[a,*] and Yixin Zhao[a,b,*]

[a] School of Environmental Science and Engineering, Shanghai Jiao Tong University, Shanghai, 200240 (China)

[b] State Key Lab of Metal Matrix Composite, Shanghai Jiao Tong University, Shanghai, 200240 (China)

[c] School of Chemical Science and Engineering, Tongji University; Shanghai, 200240 (China)

E-mail: zfchen@tongji.edu.cn (Z.C.); qianxufang@sjtu.edu.cn (X.Q.); yixin.zhao@sjtu.edu.cn (Y.Z.)

## EXPERIMENTAL

***Chemicals.*** Nickel(II) nitrate ($Ni(NO_3)_2 \cdot 6H_2O$, 98%), sodium carbonate ($Na_2CO_3$, > 99.8%), potasium hydroxide (KOH, 99%), sulfuric acid ($H_2SO_4$, 98%), acetone ($CH_3COCH_3$, 99.8%) and methanol ($CH_3OH$, 99.8%) were obtained from China National Pharmaceutical Group Corporation. Nickel foam (NF, thickness ~0.5 mm, bulk density ~0.56 g $cm^{-3}$) was obtained from Shanxi Lizhiyuan Material of Battery Co. Ltd (China) and subjected to pre-treatment by sulfuric acid, acetone, methanol and deionized water before use. All other reagents were analytical grade and used as received. All electrolyte solutions were prepared with deionized water (18 MΩ·cm) unless stated otherwise.

***Apparatus.*** Scanning electron microscope (SEM) images were obtained using a JSM-7900F (JEOL Ltd.). The SEM images were captured at an acceleration voltage of 5 kV, while EDX spectra were acquired at an acceleration voltage of 10 kV. X-ray diffraction (XRD) analysis was conducted using a Shimadzu XRD-6100 diffractometer equipped with Cu Kα radiation, operating at 40 kV and 30 mA. The scanning rate was set at 2° per minute in 2θ, with a scanning range spanning from 20 to 70 degrees.

$^1H$ NMR spectra were recorded on a Bruker-DRX 600 MHz instrument. Samples for NMR analysis were prepared by mixing 0.5 mL of electrolyte with 0.1 mL of $D_2O$, supplemented with 10 μL of a dimethyl sulfoxide (DMSO) water solution as an internal standard. The DMSO solution was prepared by diluting 10 μL of DMSO with 10 mL of deionized water. Gas analysis and quantification of gases generated by the decoupled electrolysis system were performed using a Thermo Scientific Trace 1310 gas chromatograph (GC) equipped with a pulsed discharge detector (PDD). Helium gas served as the carrier gas.

In-situ Differential Electrochemical Mass Spectrometry (DEMS) data were collected using a QAS 100 instrument from Shanghai Linglu Instruments Co., Ltd. The setup included a mass

spectrometer connected to the electrolysis cell via inlet and outlet tubes, with pure argon (Ar) gas serving as both the purge gas and the carrier gas during electrolysis. In-situ electrochemical Raman spectroscopies were collected from a confocal Raman microscope (Invia Reflex, Renishaw, UK) combined with an electrochemical workstation (Chenhua CHI760). For high performance liquid chromatography (HPLC) analysis of products obtained from PET hydrolysate oxidation, an SPD-16 HPLC system with a UV-Vis detector (210 nm) from Shimadzu Co., Japan, was employed.

Electrochemical measurements were carried out using a CHI 760E electrochemical workstation (Chenhua Corp., Shanghai, China) with a three-electrode system comprising a working electrode, a platinum plate counter electrode, and a saturated calomel reference electrode. Potentials were reported on the RHE scale and current density was calculated based on geometric surface area. Prior to each electrochemical measurement, the platinum plate counter electrode underwent routine treatment by immersion in 1 M hydrochloric acid to remove surface impurities. All experiments were conducted at a temperature of 22 ± 2 °C.

**$Ni(OH)_2$/NF Electrodes preparation procedure.** The $Ni(OH)_2$/NF electrodes were prepared by an in-situ anodic electrodepostion method. Prior to electrochemical operation, nickel foam (NF) electrodes were sonicated in 1 M HCl solution for 15 min to remove the passivation layer of $NiO_x$ on the surface, which was subsequently followed by rinsing with deionzed water and dried in the air at 40 $^oC$. Then, the $Ni(OH)_2$ materials were prepared on NF electrode by an in-situ anodic electrodeposition method in 2 M $Na_2CO_3$ solution containing 2 mM $Ni(NO_3)_2$ at an applied potential for a certain time. The obtained electrodes were denoted as $Ni(OH)_2$/NF and used for the investigation of decoupling strategy. The mass loading of $Ni(OH)_2$ material was quantified by employing an analytical balance to measure the weight before and after electrodeposition. A mass loading of 5 mg/cm² was chosen in this study.

**Hydrolysis of PET.** Alkaline hydrolysis was conducted to depolymerize PET. Initially, approximately 0.77 g of PET powder was washed sequentially with ethanol and deionized water. The dried powder was then combined with 40 mL of 1 M KOH solution and transferred to a 50 mL Teflon-lined autoclave, which was sealed and maintained at 180 °C for 2 hours. After cooling to room temperature, the resulting solution, containing 0.1 M ethylene glycol and terephthalate, was filtered and utilized as the electrolyte for electrochemical testing and analysis.

The Faradaic efficiency for the conversion of PET hydrolysate was calculated using Eq. (1).

$$Faradaic\ Efficiency = \frac{2 \times formate\ (mol) \times 96485(C/mol)}{Total\ passed\ charge\ (C)} \times 100\% \qquad (1)$$

**Solar to chemical efficency.** STC efficiency can be calculated of individual product by knowing their applied potential, operating current, faradaic efficiency of that product and input solar power.[1, 2]

$$Solar - to - Chemical\ (STC)\ Efficiency = \frac{j \times E^{o} \times FE}{P_{in}}$$

where, $j$ is the operating current density, $E^{o}$ is the applied potential of the respective product, FE is the Faradaic efficiency of the products formed on the electrodes and $P_{in}$ is input power of solar illumination. The simulated solar irradiation intensity is 100 mW/cm$^2$.

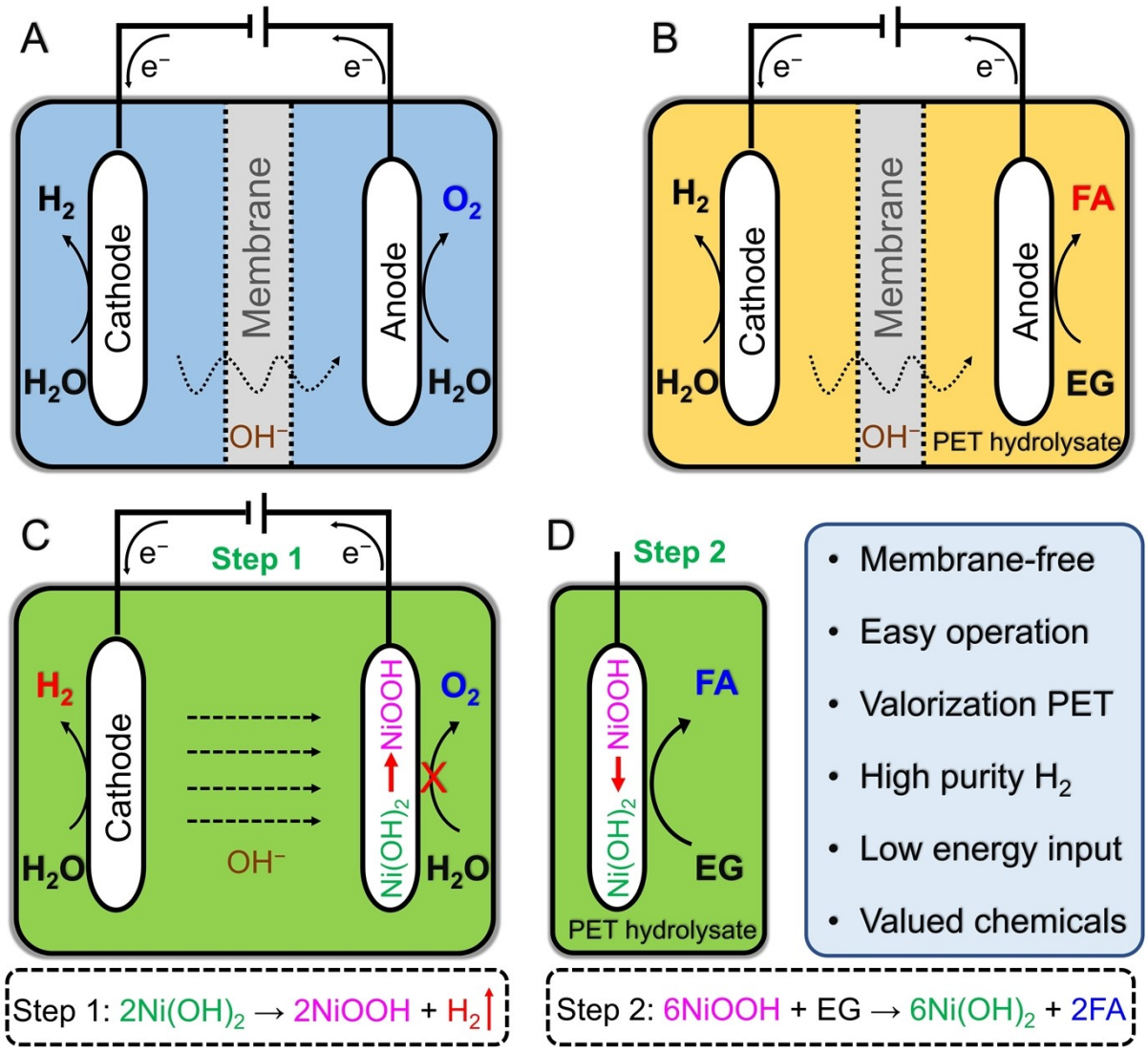


**Figure S1.** Electrolysis cell architectures. (A) Conventional configuration of an alkaline water electrolysis cell separated by the membrane. (B) The same as in A with the anodic water oxidation reaction replaced by PET hydrolysate oxidation reaction. (C, D) A schematic of the decoupling strategy by two-step operation, where step 1 involves the water reduction on the cathode ($H_2O + e^- \rightarrow H_2 + OH^-$) and the oxidation of $Ni(OH)_2$ ($Ni(OH)_2 + OH^- \rightarrow NiOOH + H_2O + e^-$). The step 1 is followed by a chemical step 2, wherein the oxidized NiOOH electrode reacts with PET hydrolysate to oxidize EG into FA and the Ni-based electrode is correspondingly reduced to the $Ni(OH)_2$.

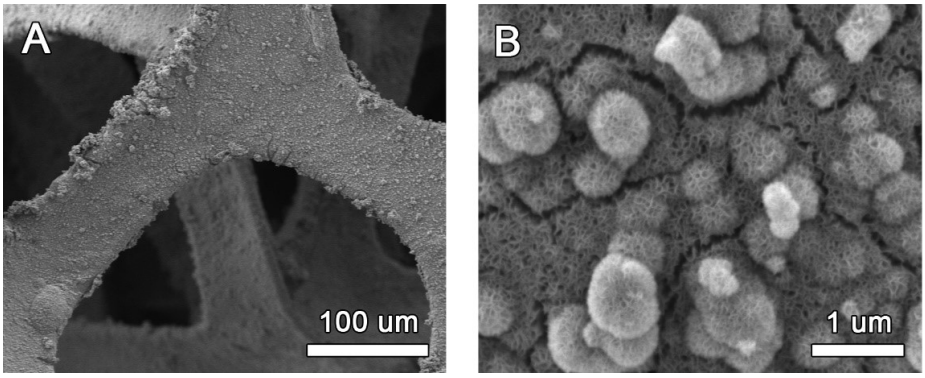


**Figure S2.** (A) SEM and (B) high-resolution SEM images of the as-prepared $Ni(OH)_2$/NF electrode.

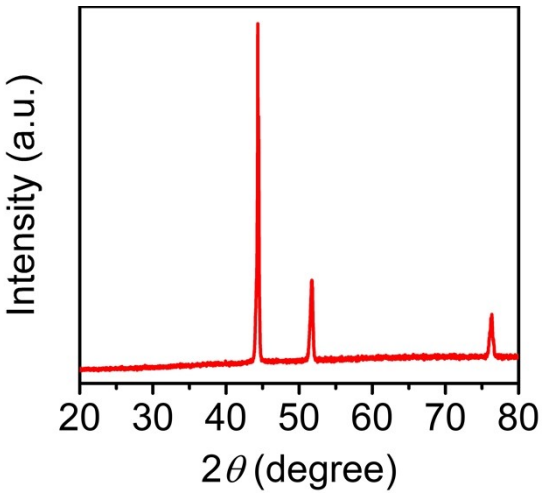


**Figure S3.** XRD pattern of the as-prepared $Ni(OH)_2$/NF electrode.

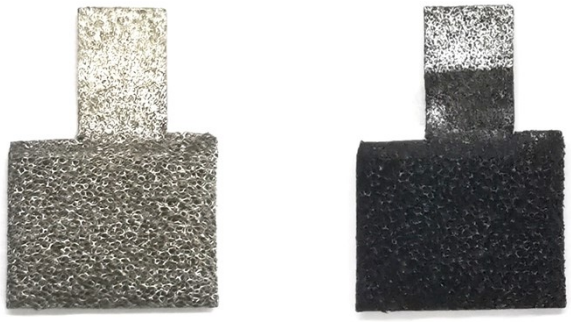

**Figure S4.** Photography of the as-prepared $Ni(OH)_2$/NF electrode and corresponding NiOOH/NF electrode.

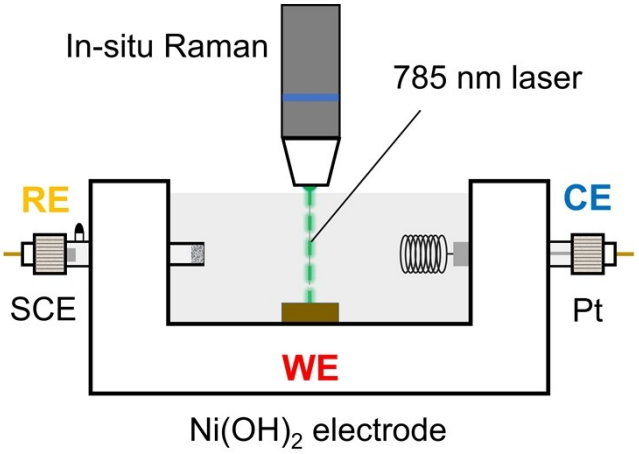


**Figure S5.** Schematic illustration of in situ Raman spectroscopy device combined with a three-electrode electrochemical system.

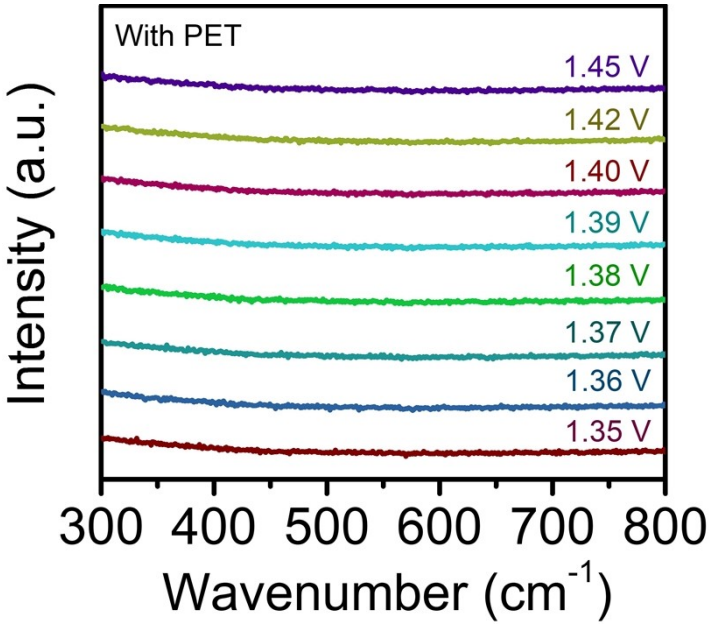


**Figure S6.** In-situ Raman spectra of $Ni(OH)_2$ electrode in 1 M KOH solution with the additional of PET hydrolysate at different potentials.

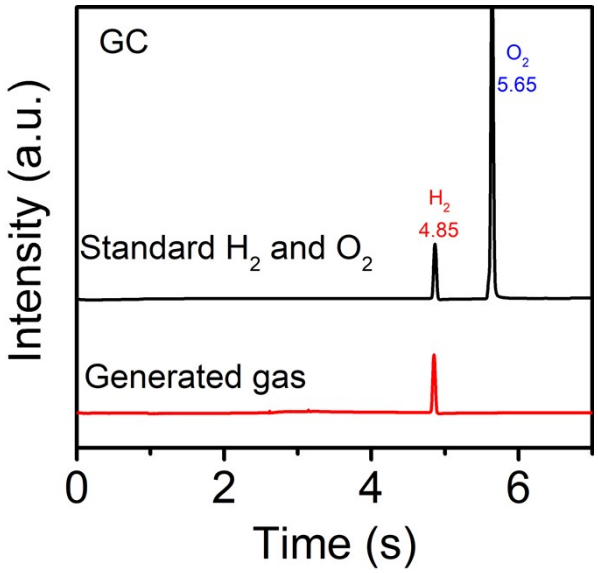


**Figure S7.** Gas Chromatogram spectra of generated gas during electrolysis and standard $H_2$ and $O_2$.

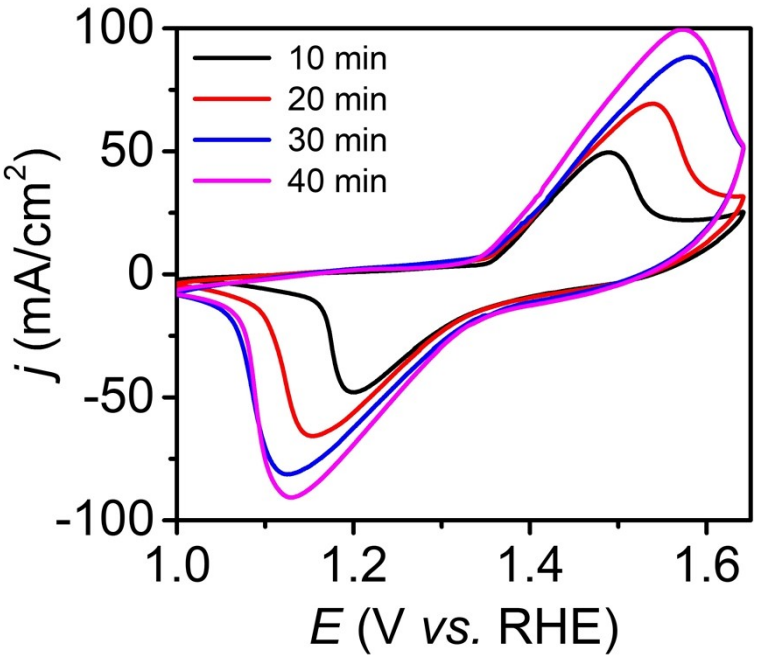


**Figure S8.** CV curves of the as-prepared $Ni(OH)_2$/NF electrode by different electro-deposition time in 1 M KOH solution at a scan rate of 10 mV/s.

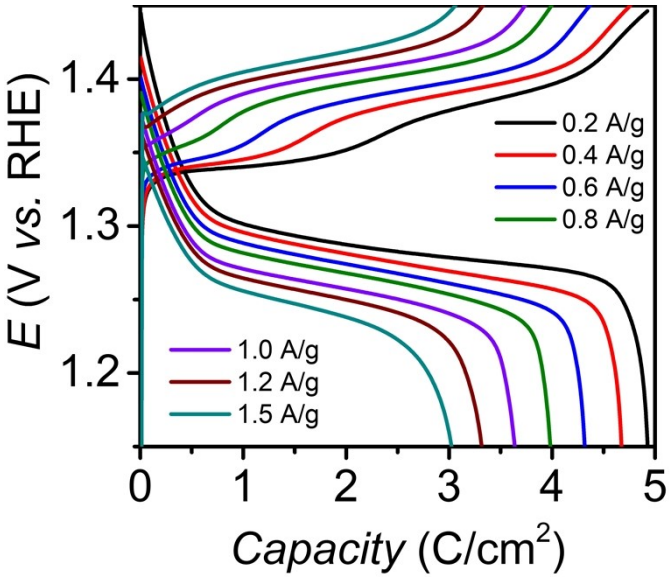


**Figure S9.** Different charging and discharging rate performance of the as-prepared $Ni(OH)_2$/NF electrode. Galvanostatic charge/discharge profiles of $Ni(OH)_2$/NF were obtained at various current densities within the voltage range of 1.05 to 1.45 V in a 1 M KOH electrolyte. The discharge capacity of $Ni(OH)_2$/NF at a current density of 0.2 A/g was found to be 5 C/cm$^2$. As the current density increased, the specific capacities of Ni(OH)2/NF exhibited a gradual decline. Remarkably, even at a high current density of 1.5 A/g, a reversible capacity of 3 C/cm$^2$ was still achieved. The mass loading of the $Ni(OH)_2$/NF electrode was approximately 5 $mg_{Ni(OH)2}$/cm$^2$.

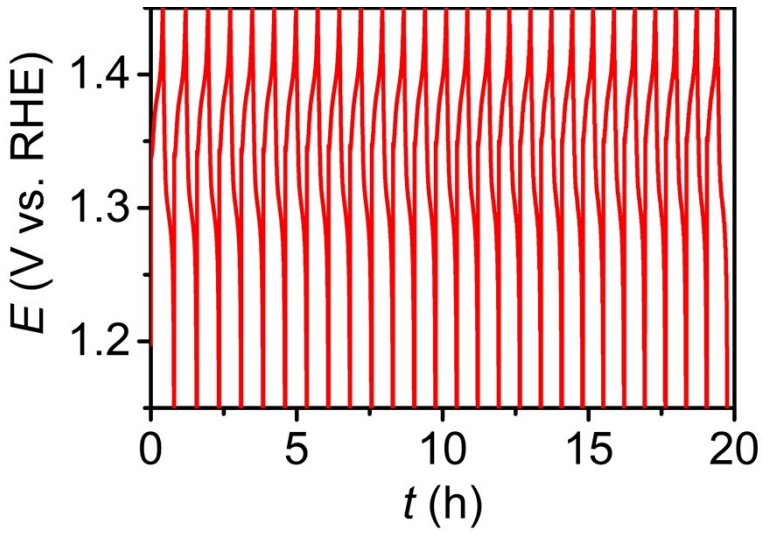


**Figure S10.** Galvanostatic charge-discharge curves of the $Ni(OH)_2$/NF electrode in 1 M KOH solution in the potential range of 1.15 V to 1.45 V for 20 h test.

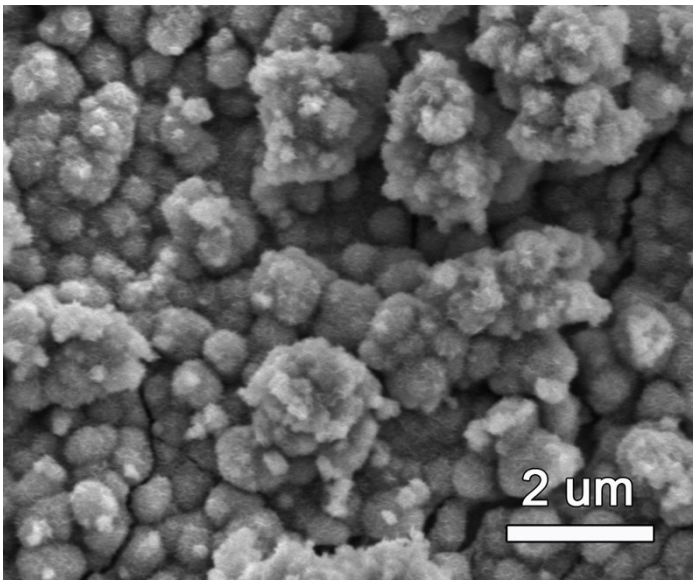


**Figure S11.** SEM image of the $Ni(OH)_2$/NF electrode after 20 h charge-discharge test.

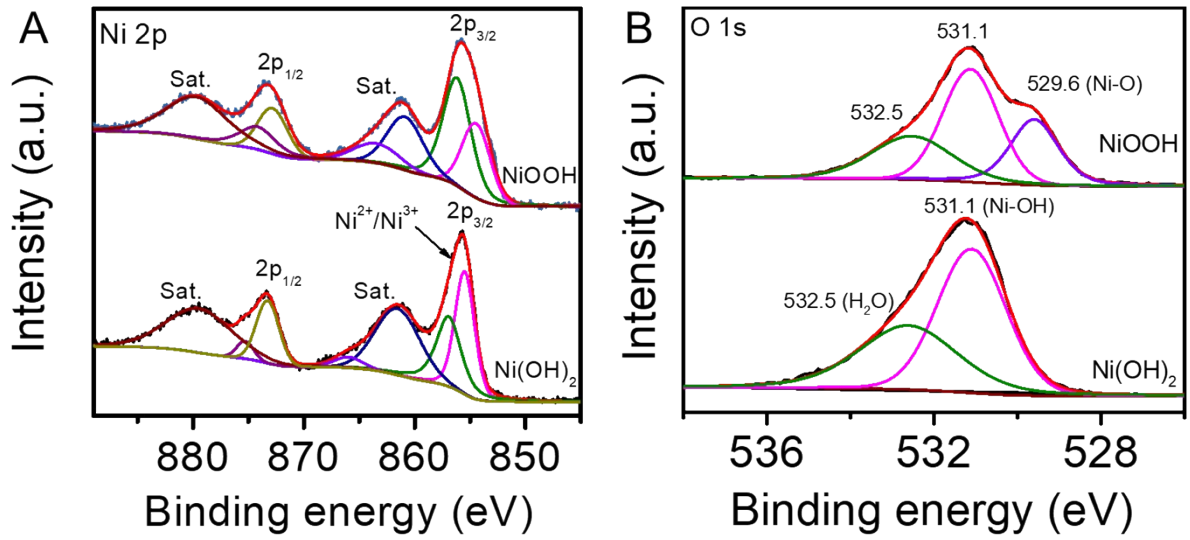


**Figure S12.** XPS spectra of (A) Ni and (B) O of the $Ni(OH)_2$/NF electrode after 20 h charge-discharge test. The results indicates that the Ni-based redox mediator electrode possess a high cycling stability, which is very important for the decoupling system.

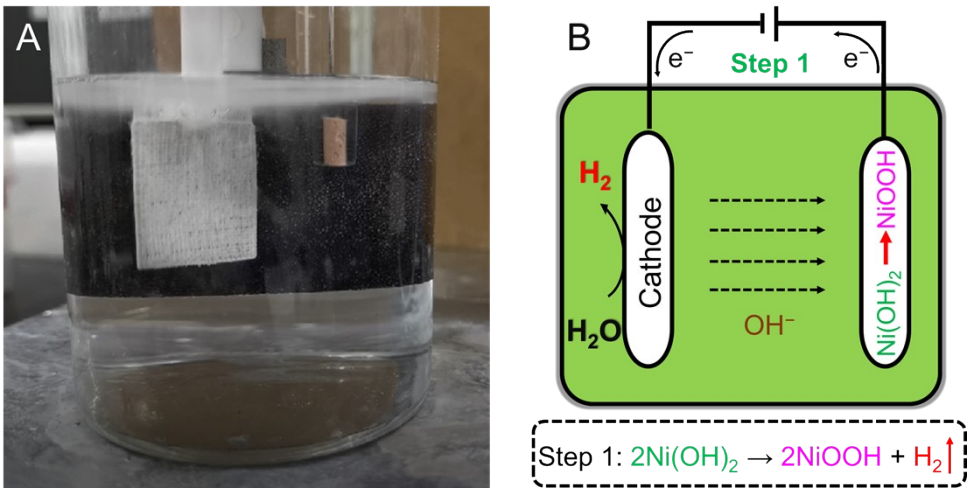


**Figure S13.** (A) Photograph of the hydrogen evolution process with assistant of $Ni(OH)_2$/NF auxiliary electrode; (B) The corresponding schematic illustration of this process.

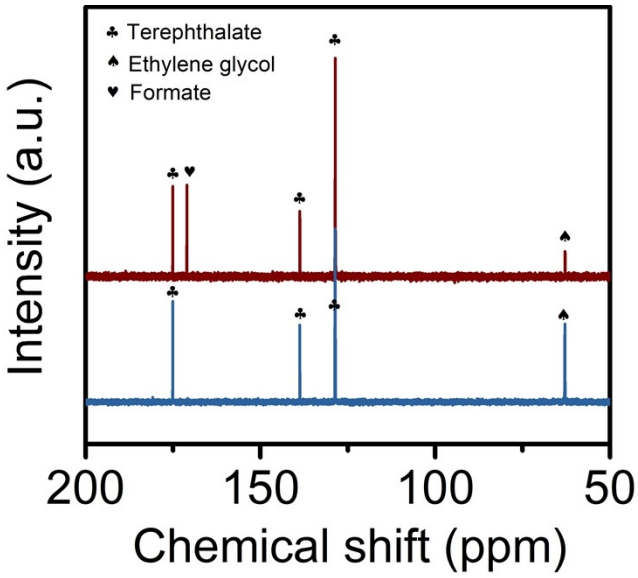


**Figure S14**. $^{13}C$ NMR spectrum of the PET hydrolysate after treated with NiOOH electrode.

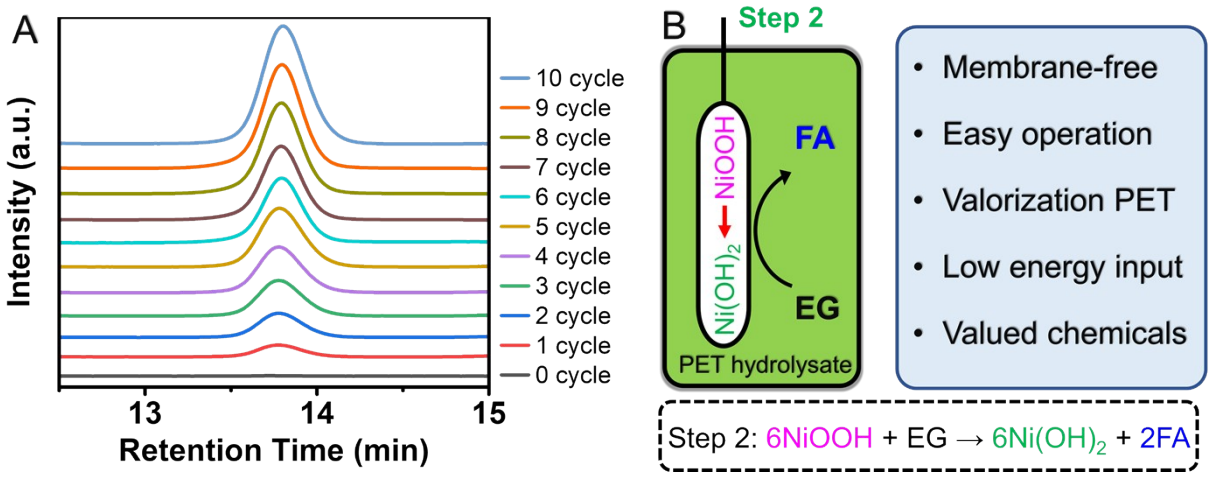


**Figure S15.** (A) HPLC chromatograms of the reaction products from the step 2 after a series of continuously immersing cycles. (B) The corresponding schematic illustration of this process.

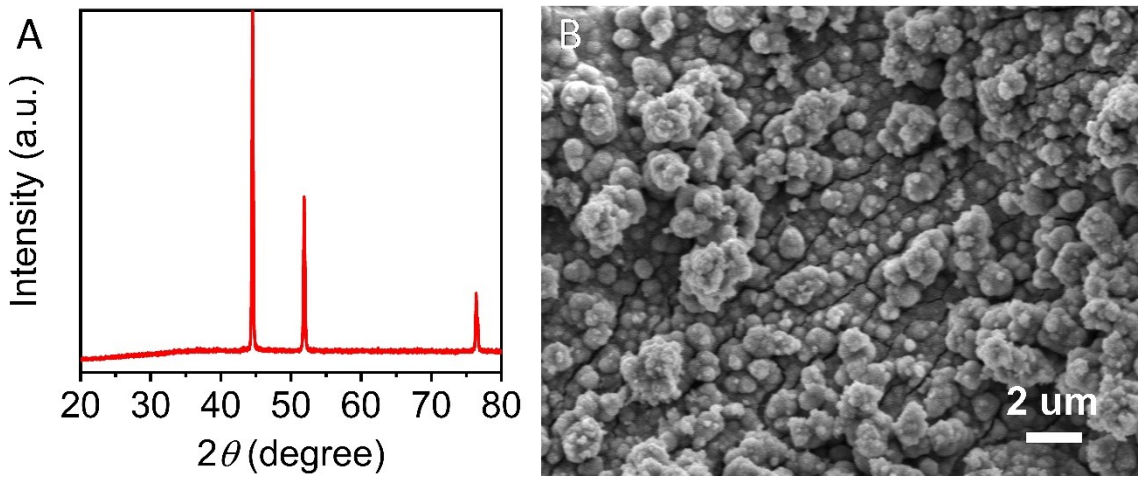


**Figure S16.** (A) XRD pattern and (B) SEM image of the $Ni(OH)_2$/NF electrode after the continuous recycling tests.

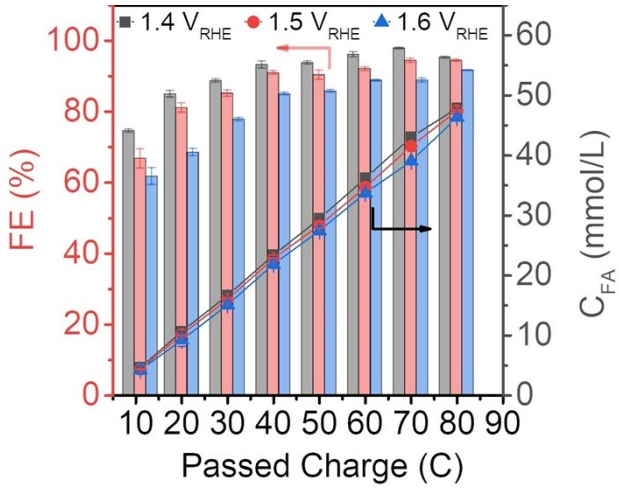


**Figure S17.** Faradaic efficiency and quantities curves for the formic acid production by $Ni(OH)_2$/NF electrode at different potential in absence of AEM in 0.1 M PET hydrolysate.

**Table S1.** Comparison of electrocatalytic performances of PET plastic wastes into formic acid product over Ni-based catalysts.

| Materials | Solution | $J$ (mA cm$^{-2}$) | $E$ ($V_{RHE}$) | Product | FE | Membrane | Ref. |
|---|---|---|---|---|---|---|---|
| $Ni(OH)_2$/NF | 1 M KOH with 0.1 M EG | 100 | 1.45 | FA | 96% | None | This Work |
| $CoNi_{0.25}P$ | 1 M KOH with 0.3 M EG | 350 | 1.7 | FA | 92% | Used | 3 |
| $NiCu_{60s}$/NF | 1 M KOH with 0.3 M EG | 100 | 1.47 | FA | 96% | Used | 4 |
| Pd-NiTe/NF | 1 M KOH with 0.5 M EG | 100 | 1.37 | FA | 96% | Used | 5 |
| $Pt_1/Ni(OH)_2$ | 1 M KOH with 0.3 M EG | 1000 | 1.444 | FA | 90% | Used | 6 |
| B,Co-NiS | 1 M KOH with 0.1 M EG | 100 | 1.341 | FA | 93% | Used | 7 |
| $Ni(OH)_2$-$V_O$ | 1 M KOH with 0.1 M EG | 300 | 1.6 | FA | 86% | Used | 8 |
| Co-$Ni_3N$/CC | 1 M KOH with 0.1 M EG | 150 | 1.3 | FA | 92% | Used | 9 |
| $Ni_{0.5}Ce_{0.5}Co_2O_4$ | 1 M KOH with 0.3 M EG | 343 | 1.55 | FA | 95% | Used | 10 |
| $Mn_{0.1}Ni_{0.9}Co_2O_{4-\delta}$ | 1 M KOH with 0.17 M EG | 50 | 1.51 | FA | 90% | Used | 11 |
| Co, Cl-NiS | 1 M KOH with 0.1 M EG | 100 | 1.346 | FA | 90% | Used | 12 |
| $Ni(OH)_2$/NF | 10 M KOH with 0.3 M EG | >500 | 1.6 | FA | 90% | Used | 13 |
| $Ni_3N/W_5N_4$ | 1 M KOH with 2 g PET | 10 | 1.33 | FA | 85% | Used | 14 |
| $NiCo_2O_4$/CFP | 1 M NaOH with 0.1 M EG | 50 | 1.42 | FA | 90% | Used | 15 |
| OMS-$Ni_1$-CoP | 1 M KOH with 0.5 M EG | 50 | 1.38 | FA | 96% | Used | 16 |

**References**


1. T. Zhang, X. Li, J. Wang, Y. Miao, T. Wang, X. Qian and Y. Zhao, *J. Hazard. Mater.*, 2023, **450**, 131054.
2. G. Gurudayal, J. Bullock, D. F. Srankó, C. M. Towle, Y. Lum, M. Hettick, M. C. Scott, A. Javey and J. Ager, *Energy Environ. Sci.*, 2017, **10**, 2222-2230.
3. H. Zhou, Y. Ren, Z. Li, M. Xu, Y. Wang, R. Ge, X. Kong, L. Zheng and H. Duan, *Nat. Commun.*, 2021, **12**, 4679.
4. H. Kang, D. He, X. Yan, B. Dao, N. B. Williams, G. I. Elliott, D. Streater, J. Nyakuchena, J. Huang, X. Pan, X. Xiao and J. Gu, *ACS Catal.*, 2024, **14**, 5314-5325.
5. H. Zhang, Y. Wang, X. Li, K. Deng, H. Yu, Y. Xu, H. Wang, Z. Wang and L. Wang, *Appl. Catal. B: Environ.*, 2024, **340**, 123236.
6. M. Song, Y. Wu, Z. Zhao, M. Zheng, C. Wang and J. Lu, *Adv. Mater.*, 2024, DOI: 10.1002/adma.202403234, e2403234.
7. Z. Chen, W. Wei, Y. Shen and B.-J. Ni, *Green Chem.*, 2023, **25**, 5979-5988.
8. F. Ma, Z. Li, R. Hu, Z. Wang, J. Wang, J. Li, Y. Nie, Z. Zheng and X. Jiang, *ACS Catal.*, 2023, **13**, 14163-14172.
9. X. Liu, Z. Fang, D. Xiong, S. Gong, Y. Niu, W. Chen and Z. Chen, *Nano Res.*, 2022, **16**, 4625-4633.
10. Z. Li, Z. Yang, S. Wang, H. Luo, Z. Xue, Z. Liu and T. Mu, *Chem. Eng. J.*, 2024, **479**, 147611.
11. Y. Mao, S. Fan, X. Li, J. Shi, M. Wang, Z. Niu and G. Chen, *J. Hazard. Mater.*, 2023, **457**, 131743.
12. Z. Chen, R. Zheng, T. Bao, T. Ma, W. Wei, Y. Shen and B. J. Ni, *Nano-Micro Lett.*, 2023, **15**, 210.
13. K. Liu, Y. Wang, F. Liu, C. Liu, R. Shi and Y. Chen, *Chem. Eng. J.*, 2023, **473**, 145292.
14. F. Ma, S. Wang, X. Gong, X. Liu, Z. Wang, P. Wang, Y. Liu, H. Cheng, Y. Dai, Z. Zheng and B. Huang, *Appl. Catal. B: Environ.*, 2022, **307**, 121198.
15. J. Wang, X. Li, M. Wang, T. Zhang, X. Chai, J. Lu, T. Wang, Y. Zhao and D. Ma, *ACS Catal.*, 2022, **12**, 6722-6728.
16. N. Wang, X. Li, M.-K. Hu, W. Wei, S.-H. Zhou, X.-T. Wu and Q.-L. Zhu, *Appl. Catal. B: Environ.*, 2022, **316**, 121667.